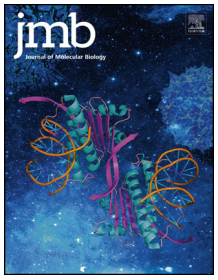

Mechanistic and Structural Origins of the Asymmetric Barrier to Prion-like Cross-Seeding between Tau-3R and Tau-4R

Harish Kumar and Jayant B. Udgaonkar

National Centre for Biological Sciences, *Tata Institute of Fundamental Research, Bengaluru 560065, India*

Correspondence to Jayant B. Udgaonkar: *Indian Institute of Science Education and Research, Pune 411008, India.*
jayant@ncbs.res.in
https://doi.org/10.1016/j.jmb.2018.09.010
Edited by Ronald Wetzel

Abstract

The spread and deposition of infectious fibrillar protein aggregates in the brain *via* a prion-like mechanism is a critical component in the patho-physiology of various neurodegenerative diseases, including the tauopathies. In tauopathies, two isoforms of tau, containing three and four microtubule binding repeats, are found to aggregate, and the type of isoform present in aggregates determines the type of tauopathy. Cross-seeding between the two tau isoforms is limited by an asymmetric barrier similar to the species barrier that restricts prion transmission across species, whose origin has remained unclear. In this study, the growth of the tau fibrils is shown to be describable by a two-step Michaelis–Menten-like model. Delineation of the mechanism as a Michaelis–Menten-like mechanism has enabled a quantitative understanding of the asymmetric seeding barrier that exists between two isoforms of tau, tau-K18 and tau-K19 (which differ in containing four and three microtubule binding repeats, respectively), wherein tau-K18 fibrils cannot seed tau-K19 monomer. Furthermore, high-resolution structural analysis of the two isoforms shows that the structural core is more ordered in tau-K19 than in tau-K18. Hence, the current work provides kinetic and structural rationales for asymmetric seeding barriers in general and for the two tau isoforms in particular.

Introduction

The spread of β-sheet-rich structured aggregates in the brain is linked to various neurodegenerative diseases, including Parkinson's disease, Alzheimer's disease, and the prion diseases [1–4]. It now appears that a prion-like mechanism [5,6], in which a specific conformation of an aggregate induces conformational conversion of the native state into an identical amyloid-like form, in a template-dependent manner, may be responsible for the propagation of aggregates of several proteins, including α-synuclein [7,8], amyloid beta [9,10] and tau [7,8,11–13].

Various misfolded forms of tau self-propagate faithfully from cell to cell and region to region in the brain and induce the misfolding and aggregation of soluble tau protein [14–18]. Tau is found in six different isoforms in the adult human brain, generated by alternative splicing of exons 2, 3, and 10 [19]. Alternative splicing of exon 10 produces tau with either three (3R) or four (4R) microtubule binding repeats [19]. The two isoforms are expressed to equal extents in the adult human brain [19]. Different tau aggregates are associated with distinct tauopathies, which comprise a group of neurodegenerative disorders with diverse clinical features [12,20–23]. In Alzheimer's disease, the isoforms tau 4R and 3R are found in the aggregates [24], whereas in progressive supranuclear palsy [25] and Pick's disease [24], only tau 4R and 3R, respectively, are found aggregated in the brain. It remains to be understood as to why either only one isoform in some cases and both isoforms in other cases aggregate. *In vitro*, it has been observed that an asymmetric seeding barrier exists between tau-K18, the four-repeat (R1, R2, R3, and R4) domain variant, and tau-K19, the three-repeat (R1, R3, and R4) domain variant of tau [26]. The barrier appears to be similar to the species barrier seen in case of prion disease, which determines the infectivity of a pathogenic prion [27,28]. The mechanistic basis of the barrier remains, however, to be understood. Obviously, an understanding of the mechanism of the template-driven conversion of soluble tau into structurally and functionally distinct types of aggregates is important for understanding the

origin of the asymmetric seeding barrier and various tauopathies.

To study the mechanism of elongation of tau fibrils, the fibrillation reaction of tau-K18 was carried out in the presence of heparin, an inducer of tau aggregation. First, the effect of seed on the fibrillation of tau-K18 was monitored by incubating 80 μM protein in the absence or presence of 2% seed, at pH 7.3 at 25 °C under quiescent solution conditions. The process of fibril formation was monitored by measuring the thioflavin T (ThT) fluorescence emission at 475 nm in a 96-well plate (Fig. 1a). Control experiments were carried out to confirm that the presence of ThT during the fibrillation reaction had no effect on the kinetics of fibril formation (Fig. S1). Heparin was used as an inducer for fibrillation; without it, tau does not aggregate within an experimentally relevant time frame even in the presence of seed (data not shown). A fixed ratio (3:4) of heparin to protein

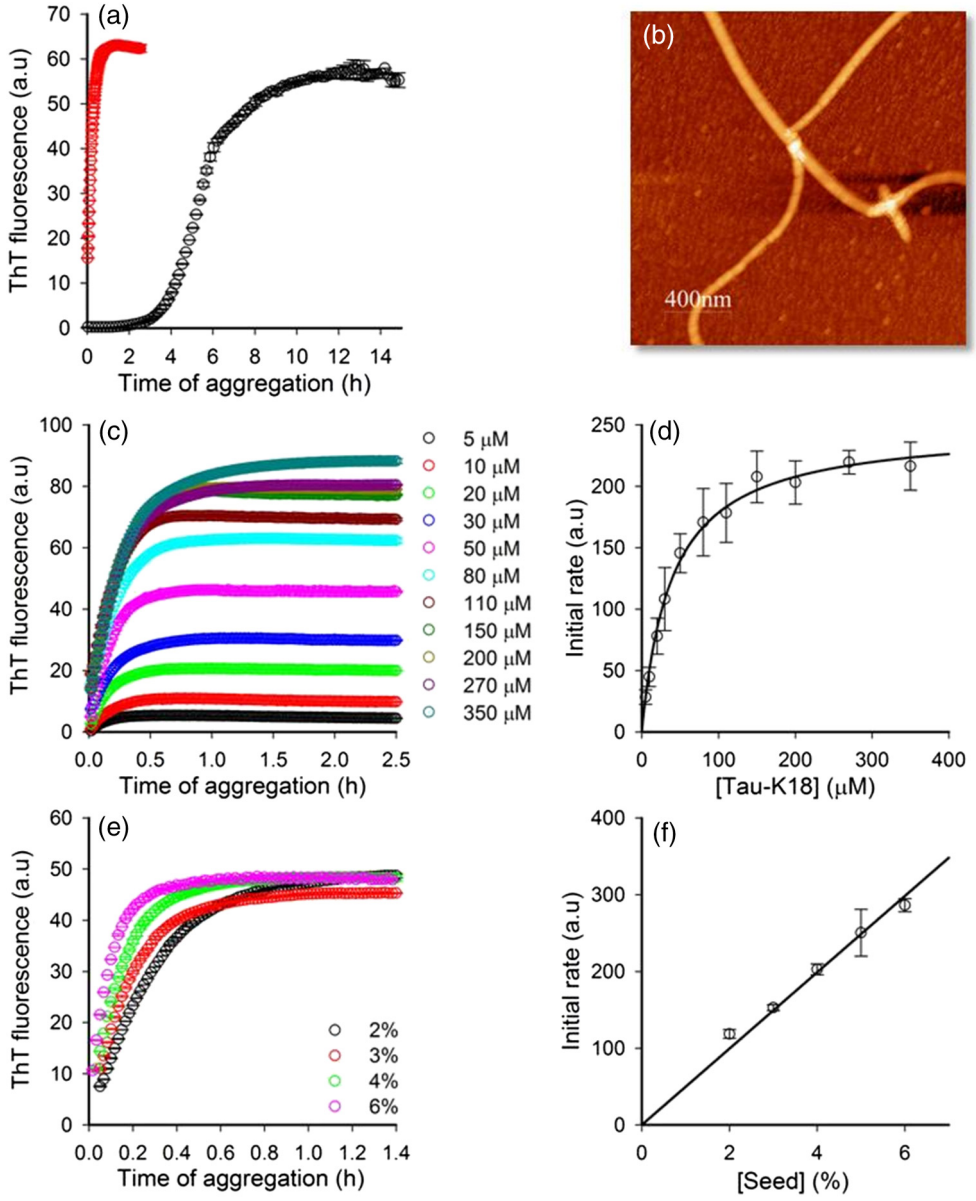

Fig. 1. Kinetics of the elongation of tau-K18 fibrils. (a) ThT fluorescence-monitored kinetics of fibril formation by 80 μM tau-K18 in the absence (black) and presence (red) of 2% seed. (b) AFM image of tau-K18 fibrils formed in the presence of seed, at saturation. (c) ThT fluorescence-monitored aggregation kinetics of tau-K18 at different monomer concentrations in the presence of 2% seed. (d) Initial rate of fibrillation (obtained by measuring the initial slopes of the kinetic curves shown in panel c) *versus* the concentration of monomeric tau-K18. (e) Aggregation kinetics of 50 μM tau-K18 at different seed concentrations. (f) Initial rate of fibrillation (determined from the kinetic curves shown in panel e) *versus* seed concentration. The error bars (in panels d and f) represent the standard deviations from three independent experiments, each with two replicates.

was used throughout the study. The dependence of fibril formation kinetics on heparin concentration was determined, and in control experiments, the kinetics was found not to vary when the heparin concentration was varied two-fold from that used in this study (Fig. S2 and SI text). In the absence of seed, fibril formation by tau-K18 followed typical sigmoidal kinetics with a lag phase of ~3-h duration (Fig. 1a). The addition of 2% tau-K18 seed abolished the lag phase and accelerated the elongation phase (Fig. 1a). The kinetics were describable as single exponential, which suggested that the concentration of seeds remained constant during the reaction. At the completion of the seeded reaction, amyloid fibrils were observed to have formed (Fig. 1a and b), and the ThT fluorescence intensity was identical to that seen for an unseeded reaction (Fig. 1a). This indicated that for both the seeded and unseeded reactions, equal amounts of monomer had converted into structurally similar fibrils. Hence, the addition of seed did not appear to affect the structure of the fibrils and equilibrium constant of the fibrillation reaction. It is important to note that the fibrillation reactions were very reproducible, and the different batches of protein monomer and seed, which had been prepared independently, gave identical results (Fig. S3).

To determine the mechanism of fibril elongation, the dependence of the initial rate of elongation of tau-K18 on soluble monomer concentration was determined at a constant concentration of preformed tau-K18 fibril/seed under pseudo-first-order conditions (Fig. 1c and d). The initial rate of fibril elongation was determined by measuring the slope of the kinetic curve using the first 5–6 data points (Fig. 1c and d). At lower monomer concentrations, the initial rate shows a linear dependence on monomer concentration. This is expected when the fibril end grows by the addition of monomers and when the diffusion of monomers to the fibril ends is the rate-limiting step. The observation also suggests that it is unlikely that fibrils grow by oligomer addition to the fibril ends. In fact, oligomers are not seen in atomic force microscopy (AFM) images of aggregating protein at the initial time points (Fig. S4). The initial rate of fibril growth was found to be proportional directly to the seed concentration (Fig. 1e and f), which is expected because an increase in the seed concentration provides proportionately more fibril ends to which monomers can add. In earlier studies, fibrils formed by both the yeast prion protein [29] and α-synuclein [30] were shown to grow in a similar manner. At higher monomer concentrations, the initial rate was found to become independent of monomer concentration, suggesting that a first-order process such as a conformational transition had become the rate-limiting step and that the diffusion of monomer to the fibril ends was no longer rate-limiting.

The nonlinear dependence of the initial rate of fibril elongation on monomer concentration (Fig. 1d) is suggestive of the Michaelis–Menten (MM) kinetics observed commonly for enzyme-catalyzed reactions. It seems that an MM-like mechanism can explain the kinetics of elongation, with the soluble monomer being the substrate and with the fibril ends playing the role of catalyst. In such a mechanism, the concentration of catalyst would remain constant, as the catalyst is present at the fibril ends, and the fibrils increase only in length and not in the number. The concentration of substrate would remain in excess of the concentration of catalyst, as the number concentration of tau-K18 monomers is much higher than that of fibril seeds.

Such a mechanism is describable as:

$$F + M \underset{k_{-1}}{\overset{k_1}{\rightleftarrows}} F.M \xrightarrow{k_{conv.}} FF$$

where F is the fibril seed, M is the tau-K18 monomer, F.M is the bound complex in which the monomer is yet to be conformationally converted, and FF is the converted fibril which again acts as a seed (enzyme).

Fibril formation is a complex reaction, and various processes like primary and secondary nucleation, growth and dissociation of nuclei and fibrils determine/influence the kinetics of fibril formation [31]. Before analyzing the fibril formation reaction of tau according to a simple MM-like mechanism, it was important to show that the concentration of fibrils, which serve as the "enzyme," remained constant during the reaction. Two experimental approaches were utilized to show that the number concentration of fibrils/fibril ends did not vary. In one approach, AFM was used to count the number of fibrils at different times during the fibril formation/elongation reaction (Fig. 2a and b). Figure 2c and d shows that the number of fibrils did, indeed, not increase with time of reaction. In the second approach, fibrils formed at early times of aggregation were quantified by an amyloid chain reaction assay, which is a very sensitive method for quantifying fibril concentration [32]. It was found that when aliquots were withdrawn at different early times from an aggregating protein solution and used to seed fibril formation in a fresh monomer solution, the kinetics of the seeded fibril formation reaction did not vary with the time at which the seed had been withdrawn (Fig. 2e and f). This clearly indicated that the concentration of fibrils at the early time points did not change with time of aggregation. Hence, a basic tenet of an MM-like mechanism appears to hold true, namely, that the concentration of fibrils (which act as the enzyme) does not vary during the course of the reaction.

For an MM-like mechanism, the maximum rate of conformation conversion, V_{max}, and the value of K_m, the protein concentration at which the initial rate of reaction is $V_{max}/2$, are easily determined from the dependence of the initial rate on monomer concentration. K_m and V_{max} are good measures of the affinity between monomer and fibril end, and of the rate constant with which monomer converts into the β-sheet-rich amyloid form, respectively. These

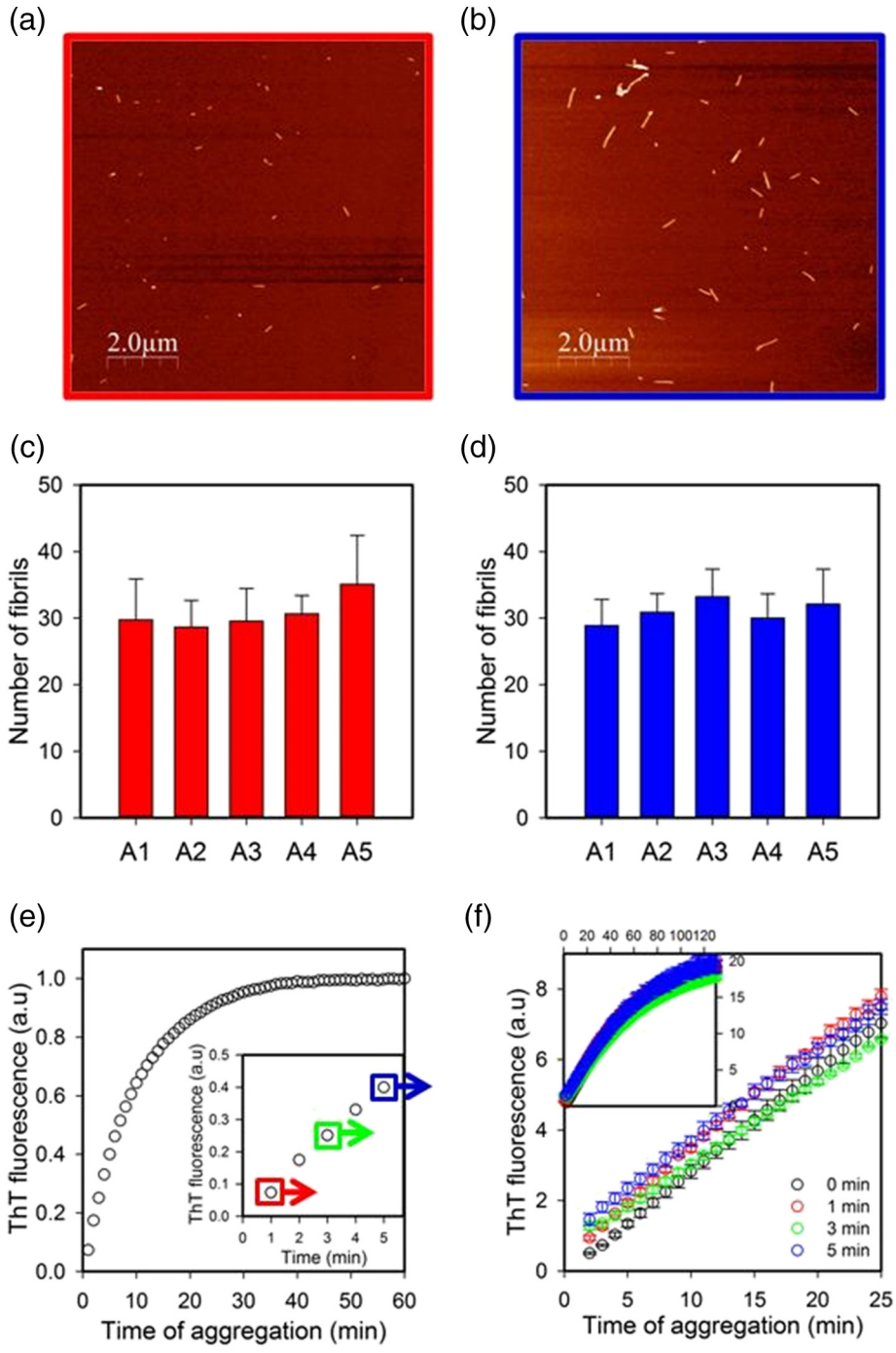

Fig. 2. Concentration of seed remains constant during the seeding reaction. AFM image of fibrils formed by 20 μM tau-K19 in the presence of 2% seed at (a) 1 min and (b) 5 min of aggregation. Number of fibrils formed at (c) 1 min and (d) 5 min. AFM images were acquired at five random places on the mica. The error bars represent the standard deviations from counting nine equally sized square areas in each AFM image. (e) ThT fluorescence-monitored kinetics of 20 μM tau-K18 in the presence of 2% seed. The inset shows the initial phase of the reaction. (f) At three initial time points (shown in panel e), a 100-μl reaction aliquot was withdrawn and was added to a solution of fresh 20 μM monomer. The aggregation kinetics was then monitored by ThT fluorescence.

parameters K_m and V_{max} can be used to quantitatively compare the elongation kinetics of the different types of fibrils by the two variants of tau, tau-K18 and tau-K19.

To this end, the fibril elongation reactions of tau-K18 and tau-K19 were studied. The fibrillation of tau-K18 and tau-K19 was carried out in the presence of both

tau-K18 and tau-K19 seeds (Fig. 3a and b). Tau-K18 seeds were found to be capable of seeding tau-K18 monomers, but not tau-K19 monomers (Fig. 3a and b). Interestingly, tau-K19 seeds were found to be capable of seeding both tau-K19 and tau-K18 monomers (Fig. 3a and b), forming fibrils of similar morphology (Fig. S5). Hence, the cross-seeding experiments confirmed the existence of an asymmetric seeding barrier between the morphologically similar fibrils of tau-K18 and tau-K19. This is probably due to the incompatibility between tau-K19 monomers and tau-K18 fibril ends.

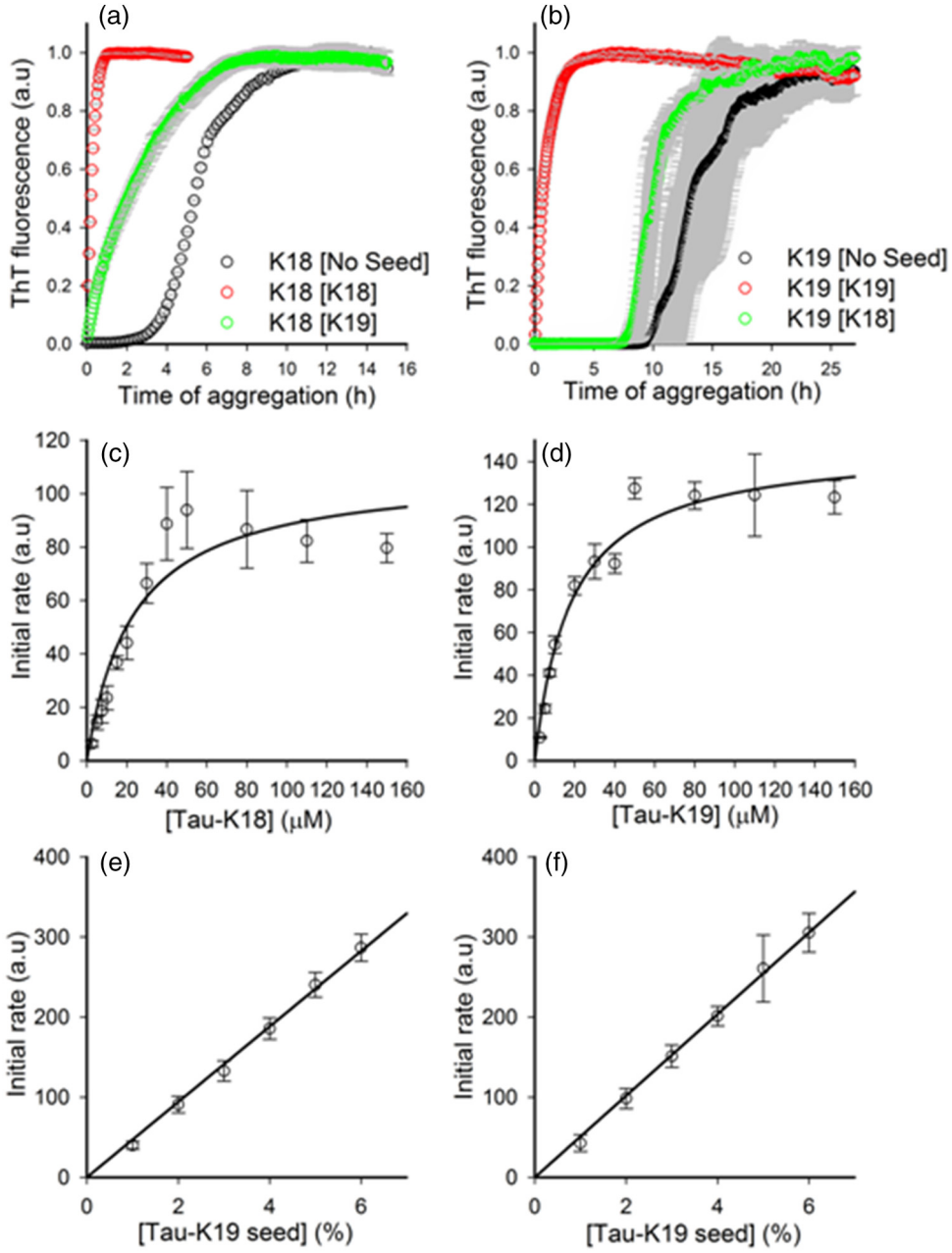

Fig. 3. Existence of an asymmetric seeding barrier between the seeding of tau-K18 and tau-K19, and kinetics of the elongation of tau-K19 fibrils. (a) ThT fluorescence-monitored kinetics of fibril formation by tau-K18 in the absence and presence of 2% seed. (b) ThT fluorescence-monitored kinetics of fibril formation by tau-K19 in the absence and presence of 2% seed. In panels a and b, the nature of the seed is shown inside the square brackets. (c) Initial rate of fibril formation by monomeric tau-K18 in the presence of 2% tau-K19 seed *versus* monomer concentration. (d) Initial rate of fibril formation by monomeric tau-K19 in the presence of 2% tau-K19 seed *versus* monomer concentration. Initial rate of fibril formation by 50 μM monomeric (e) tau-K18 and (f) tau-K19 *versus* seed concentration. The error bars (in panel c–f) represent the standard deviations from three independent experiments each with two replicates.

To find the extent of compatibility, the catalytic efficiencies of tau-K18 and tau-K19 seeds were compared for tau-K18 monomer, which is analogous to comparing two different enzymes catalyzing the reaction of same substrate. For that, fibrillation of tau-K18 monomer at different concentrations was carried out independently in the presence of tau-K18 and tau-K19 seed (Figs. 1d and 3c). K_m and V_{max} were obtained for both the reactions by fitting the data (dependence of the initial rate on monomer concentration) to an MM-like model (Figs. 1d and 3c, Table 1). The data suggest that tau-K18 monomer binds to tau-K19 seed with about 2-fold higher affinity than to tau-K18 seed; however, tau-K18 seed catalyzed the conformational transition of monomer (F.M → FF, in the mechanism shown above) about 2.5-fold faster than tau-K19 seed.

The catalytic efficiency of tau-K19 seed was compared for tau-K18 monomer and tau-K19 monomer. This is analogous to the same enzyme catalyzing the reactions of two different substrates. From the values of K_m and V_{max} (Fig. 3c and d, Table 1), it appears that tau-K19 seed binds to both isoforms with similar affinities. V_{max} was, however, about 1.5-fold higher for tau-K19 monomer. The initial rate of fibril growth (tau-K19 seed) was directly proportional to the seed concentration at constant monomer concentration for each isoform of tau protein (Fig. 3e and f).

To determine why tau-K18 and tau-K19 fibrils grow at dramatically different rates despite having similar external morphologies (Fig. 1b and S5), it became necessary to examine their internal structures. The structural core of tau-K18 and tau-K19 fibrils has been shown by solid-state NMR [33,34], cryo-electron microscopy [35,36], electron paramagnetic resonance [37,38], hydrogen–deuterium exchange (HDX) NMR [33], and HDX mass spectrometry (HDX-MS) [39], to be formed by R3 and at least part of, if not all of, R4 [33–41]. The infrared spectra (Fig. 4a) of the fibrils made by tau-K18 and tau-K19 showed a difference in the absorbance near 1650 cm^{-1} (Fig. 4a) and indicate that tau-K18 fibrils possess more disordered structure than tau-K19 fibrils. HDX-MS was used to further characterize the difference in the internal structures of the fibrils. A peptide map of tau-K18 and tau-K19 was generated (Fig. S6). In HDX-MS studies, sequence segments that are in structured β-sheet would show strong protection and would show very little deuterium incorporation upon labeling, whereas sequence segments that are disordered would get labeled to the same extent as in monomer. Interestingly, sequence segments spanning residues 258–268 and 316–357 were found to be more protected for tau-K19 than for tau-K18 fibrils (Fig. 4b, c and S7). The higher protection indicates an increase in ordered structure, or an expansion of the structural core.

The strongly protected residues in R3 span sequence segment 309–315 and in R4 span sequence segment 309–346. Two-thirds of R3 and one-third of R4 (sequence segment 316–346) are more strongly protected in tau-K19 fibrils than in tau-K18 fibrils, suggesting that the conformation of most of R3 and one-third of R4 in the fibril is less ordered when R2 is present than when it is absent. Consequently, when R2 is present in the fibril, it would appear that the interaction between R3 in the fibril and in the monomer is too weak for monomer to bind to fibril. The sequence segment spanning residues 285–307 (in R2), which is absent in tau-K19, was found to be strongly protected for tau-K18 (Fig. 4b, c and S7). It seems that for monomer to bind to fibril containing both R2 and R3, as in the case of tau-K18, the monomer itself must contain R2. It seems that the R2 (monomer)–R2 (fibril) interaction energy adds on to the weak R3 (monomer)–R3 (fibril) interaction energy, so that monomer addition can occur. The absence of a compatible fibrillar R3 conformation for monomer addition in a pool of various polymorphs can provide an explanation for the observed asymmetric seeding barrier. It should be pointed out that cryo-electron microscopy studies [35,36] of fibrils formed by full-length tau indicate that the fibril core not only includes R3 and R4, as also suggested by solid-state NMR studies [34], but also extends 10 residues beyond R4. The last six of these core residues are not present in the tau-K18 and tauK19 variants studied here. In future studies of fibrils formed by full length tau, it will be important to determine whether the last six residues of the fibril core play any role in the asymmetric seeding barrier.

Table 1. Kinetic parameters governing the fibril formation reaction of different variants of tau

Monomer [seed]	K_m (μM)	V_{max}
K18 [K18]	37.5 ± 9.5	249 ± 15
K19 [K19]	18.4 ± 3.2	148 ± 09
K18 [K19]	23.4 ± 3.8	109 ± 11

The values of K_m and V_{max} were obtained from analyzing the data in Figs. 1 and 3, according to an MM-like mechanism.

Conclusions

This study demonstrates the applicability of a simple model for understanding the molecular mechanism of template-driven fibril growth. Fibril growth is shown to follow a simple MM-like two-step model in which monomers act like the substrate and growing seeds (fibrils) act like the enzyme. This model is consistent with a “dock-lock” mechanism proposed for addition of monomer to the fibril ends [29,30,42–45]. Modeling the tau fibril formation reaction to a simple MM-like model provides a mechanistic rationale for the asymmetric seeding barrier, which exists between two isoforms of the tau protein. This study shows that fibrils of tau-K18 and tau-K19 are structurally different and that the

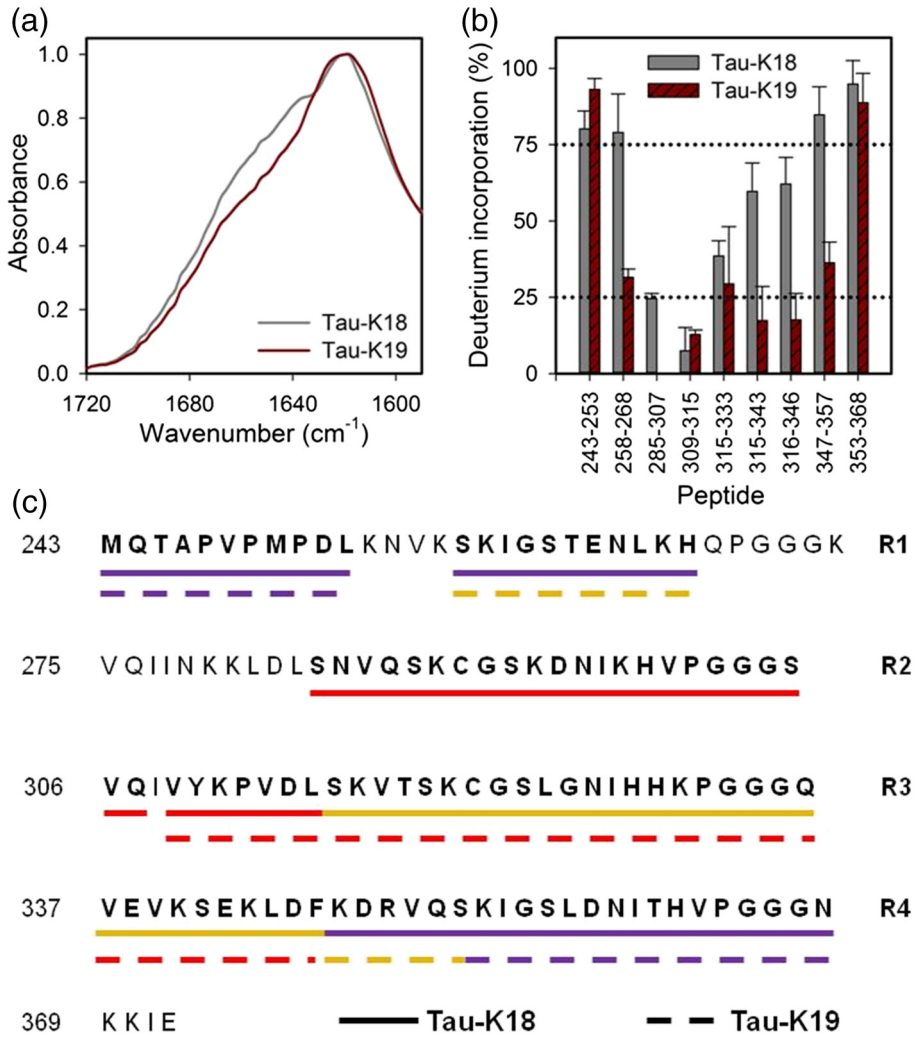

Fig. 4. Differences in the structural core of fibrils formed by tau-K18 and tau-K19. (a) FTIR spectra. (b) The percent deuterium incorporation into different sequence segments of tau-K18 (dark gray) and tau-K19 (dark red) fibrils. The dotted lines represent the 25% and 75% deuterium incorporation. The error bars represent the standard deviations from two independent experiments each with two replicates. (c) HDX protection map of tau-K18 (solid line) and tau-K19 fibrils (dashed line). The colors represent the level of deuterium incorporation: (<25% D) strongly protected (red), (25%–75% D) moderately protected (yellow), (>75% D) weakly protected (purple). Note that R2 is absent in tau-K19.

structure of the fibril dictates its seeding specificity. The simple MM-like model can be used as a quantitative tool to identify and compare different fibrillar strains of tau, in order to obtain greater insight into the link between the different strains and various tauopathies, which will help in the development of new therapeutics.

Acknowledgments

We thank members of our laboratory, as well as Jogender Singh, M.K. Mathew, and S. Gosavi, for discussion and for their comments on the manuscript. We thank Prashant Jethva for assistance in carrying out the HDX-MS experiments. The AFM images were collected at the Central Imaging and Flow Facility of the National Centre for Biological Sciences. J.B.U. is a recipient of a JC Bose National Fellowship from the Government of India. This work was funded by the Tata Institute of Fundamental Research and by the Department of Biotechnology, Government of India.

Appendix A. Supplementary data

Supplementary data to this article can be found online at https://doi.org/10.1016/j.jmb.2018.09.010.

Received 9 July 2018;
Received in revised form 4 September 2018;
Accepted 12 September 2018
Available online 26 September 2018

Keywords:
neurodegenerative disease;
kinetics;
hydrogen–deuterium exchange mass spectrometry;
tau fibrils

Abbreviations used:
HDX, hydrogen–deuterium exchange; MS, mass spectrometry; ThT, thioflavin T; AFM, atomic force microscopy.

References

[1] M.G. Spillantini, M.L. Schmidt, V.M. Lee, J.Q. Trojanowski, R. Jakes, M. Goedert, Alpha-synuclein in Lewy bodies, Nature 388 (1997) 839–840, https://doi.org/10.1038/42166.
[2] M. Goedert, Alpha-synuclein and neurodegenerative diseases, Nat. Rev. Neurosci. 2 (2001) 492–501, https://doi.org/10.1038/35081564.
[3] M. Stefani, C.M. Dobson, Protein aggregation and aggregate toxicity: new insights into protein folding, misfolding diseases and biological evolution, J. Mol. Med. (Berl). 81 (2003) 678–699, https://doi.org/10.1007/s00109-003-0464-5.
[4] J. Safar, H. Wille, V. Itri, D. Groth, H. Serban, M. Torchia, F.E. Cohen, S.B. Prusiner, Eight prion strains have PrP(Sc) molecules with different conformations, Nat. Med. 4 (1998) 1157–1165, https://doi.org/10.1038/2654.
[5] K. Marciniuk, R. Taschuk, S. Napper, Evidence for prion-like mechanisms in several neurodegenerative diseases: potential implications for immunotherapy, Clin. Dev. Immunol. 2013 (2013), 473706. https://doi.org/10.1155/2013/473706.
[6] J. Collinge, A.R. Clarke, A general model of prion strains and their pathogenicity, Science 318 (2007) 930–936, https://doi.org/10.1126/science.1138718.
[7] M. Jucker, L.C. Walker, Self-propagation of pathogenic protein aggregates in neurodegenerative diseases, Nature 501 (2013) 45–51, https://doi.org/10.1038/nature12481.
[8] M. Masuda-Suzukake, T. Nonaka, M. Hosokawa, T. Oikawa, T. Arai, H. Akiyama, D.M.A. Mann, M. Hasegawa, Prion-like spreading of pathological α-synuclein in brain, Brain 136 (2013) 1128–1138, https://doi.org/10.1093/brain/awt037.
[9] A.T. Petkova, R.D. Leapman, Z. Guo, W.-M. Yau, M.P. Mattson, R. Tycko, Self-propagating, molecular-level polymorphism in Alzheimer's beta-amyloid fibrils, Science 307 (2005) 262–265, https://doi.org/10.1126/science.1105850.
[10] M. Meyer-Luehmann, J. Coomaraswamy, T. Bolmont, S. Kaeser, C. Schaefer, E. Kilger, A. Neuenschwander, D. Abramowski, P. Frey, A.L. Jaton, J.-M. Vigouret, P. Paganetti, D.M. Walsh, P.M. Mathews, J. Ghiso, M. Staufenbiel, L.C. Walker, M. Jucker, Exogenous induction of cerebral beta-amyloidogenesis is governed by agent and host, Science 313 (2006) 1781–1784, https://doi.org/10.1126/science.1131864.
[11] F. Clavaguera, T. Bolmont, R.A. Crowther, D. Abramowski, S. Frank, A. Probst, G. Fraser, A.K. Stalder, M. Beibel, M. Staufenbiel, M. Jucker, M. Goedert, M. Tolnay, Transmission and spreading of tauopathy in transgenic mouse brain, Nat. Cell Biol. 11 (2009) 909–913, https://doi.org/10.1038/ncb1901.
[12] D.W. Sanders, S.K. Kaufman, S.L. Devos, A.M. Sharma, H. Mirbaha, A. Li, S.J. Barker, A.C. Foley, J.R. Thorpe, L.C. Serpell, T.M. Miller, L.T. Grinberg, W.W. Seeley, M.I. Diamond, Distinct tau prion strains propagate in cells and mice and define different tauopathies, Neuron 82 (2014) 1271–1288, https://doi.org/10.1016/j.neuron.2014.04.047.
[13] M. Goedert, NEURODEGENERATION. Alzheimer's and Parkinson's diseases: the prion concept in relation to assembled Aβ, tau, and α-synuclein, Science 349 (2015) 1255555, https://doi.org/10.1126/science.1255555.
[14] B. Frost, J. Ollesch, H. Wille, M.I. Diamond, Conformational diversity of wild-type tau fibrils specified by templated conformation change, J. Biol. Chem. 284 (2009) 3546–3551, https://doi.org/10.1074/jbc.M805627200.
[15] B.B. Holmes, J.L. Furman, T.E. Mahan, T.R. Yamasaki, H. Mirbaha, W.C. Eades, L. Belaygorod, N.J. Cairns, D.M. Holtzman, M.I. Diamond, Proteopathic tau seeding predicts tauopathy *in vivo*, Proc. Natl. Acad. Sci. U.S.A. 111 (2014) 4376–4385.
[16] N. Kfoury, B.B. Holmes, H. Jiang, D.M. Holtzman, M.I. Diamond, Trans-cellular propagation of Tau aggregation by fibrillar species, J. Biol. Chem. 287 (2012) 19440–19451, https://doi.org/10.1074/jbc.M112.346072.
[17] B.B. Holmes, M.I. Diamond, Prion-like properties of Tau protein: the importance of extracellular Tau as a therapeutic target, J. Biol. Chem. 289 (2014) 19855–19861, https://doi.org/10.1074/jbc.R114.549295.
[18] F. Clavaguera, F. Grueninger, M. Tolnay, Intercellular transfer of tau aggregates and spreading of tau pathology: implications for therapeutic strategies, Neuropharmacology 76 (Pt A) (2014) 9–15, https://doi.org/10.1016/j.neuropharm.2013.08.037.
[19] M. Goedert, M.G. Spillantini, R. Jakes, D. Rutherford, R.A. Crowther, Multiple isoforms of human microtubule-associated protein tau: sequences and localization in neurofibrillary tangles of Alzheimer's disease, Neuron 3 (1989) 519–526, https://doi.org/10.1016/0896-6273(89)90210-9.
[20] V.M.-Y. Lee, M. Goedert, J.Q. Trojanowski, Neurodegenerative tauopathies, Annu. Rev. Neurosci. 24 (2001) 1121–1159, https://doi.org/10.1146/annurev.neuro.24.1.1121.
[21] F. Hernández, J. Avila, Tauopathies, Cell. Mol. Life Sci. 64 (2007) 2219–2233, https://doi.org/10.1007/s00018-007-7220-x.
[22] M. Goedert, M.G. Spillantini, Propagation of tau aggregates, Mol. Brain 10 (2017), 18. https://doi.org/10.1186/s13041-017-0298-7.
[23] M. Morris, S. Maeda, K. Vossel, L. Mucke, The many faces of tau, Neuron 70 (2011) 410–426, https://doi.org/10.1016/j.neuron.2011.04.009.
[24] A. Delacourte, N. Sergeant, A. Wattez, D. Gauvreau, Y. Robitaille, Vulnerable neuronal subsets in Alzheimer's and Pick's disease are distinguished by their tau isoform distribution and phosphorylation, Ann. Neurol. 43 (1998) 193–204, https://doi.org/10.1002/ana.410430209.
[25] N. Sergeant, A. Wattez, A. Delacourte, Neurofibrillary degeneration in progressive supranuclear palsy and corticobasal degeneration: Tau pathologies with exclusively "exon 10" isoforms, J. Neurochem. 72 (1999) 1243–1249, https://doi.org/10.1046/j.1471-4159.1999.0721243.x.
[26] P.D. Dinkel, A. Siddiqua, H. Huynh, M. Shah, M. Margittai, Variations in filament conformation dictate seeding barrier between three- and four-repeat tau, Biochemistry 50 (2011) 4330–4336, https://doi.org/10.1021/bi2004685.
[27] A.F. Hill, M. Desbruslais, S. Joiner, K.C.L. Sidle, I. Gowland, J. Collinge, L.J. Doey, P. Lantos, The same prion strain

causes vCJD and BSE, Nature 389 (1997) 448–450 , 526 https://doi.org/10.1038/38925.
[28] M.E. Bruce, R.G. Will, J.W. Ironside, I. McConnell, D. Drummond, A. Suttie, L. McCardle, A. Chree, J. Hope, C. Birkett, S. Cousens, H. Fraser, C.J. Bostock, Transmissions to mice indicate that "new variant" CJD is caused by the BSE agent, Nature 389 (1997) 498–501, https://doi.org/10.1038/39057.
[29] S.R. Collins, A. Douglass, R.D. Vale, J.S. Weissman, Mechanism of prion propagation: amyloid growth occurs by monomer addition, PLoS Biol. 2 (2004), e321. https://doi.org/10.1371/journal.pbio.0020321.
[30] A.K. Buell, C. Galvagnion, R. Gaspar, E. Sparr, M. Vendruscolo, T.P.J. Knowles, S. Linse, C.M. Dobson, Solution conditions determine the relative importance of nucleation and growth processes in α-synuclein aggregation, Proc. Natl. Acad. Sci. U. S. A. 111 (2014) 7671–7676, https://doi.org/10.1073/pnas.1315346111.
[31] G. Meisl, J.B. Kirkegaard, P. Arosio, T.C.T. Michaels, M. Vendruscolo, C.M. Dobson, S. Linse, T.P.J. Knowles, Molecular mechanisms of protein aggregation from global fitting of kinetic models, Nat. Protoc. 11 (2016) 252–272, https://doi.org/10.1038/nprot.2016.010.
[32] P. Arosio, R. Cukalevski, B. Frohm, T.P.J. Knowles, S. Linse, Quantification of the concentration of Aβ42 propagons during the lag phase by an amyloid chain reaction assay, J. Am. Chem. Soc. 136 (2014) 219–225, https://doi.org/10.1021/ja408765u.
[33] V. Daebel, S. Chinnathambi, J. Biernat, M. Schwalbe, B. Habenstein, A. Loquet, E. Akoury, K. Tepper, H. Müller, M. Baldus, C. Griesinger, M. Zweckstetter, E. Mandelkow, V. Vijayan, A. Lange, β-Sheet core of tau paired helical filaments revealed by solid-state NMR, J. Am. Chem. Soc. 134 (2012) 13982–13989, https://doi.org/10.1021/ja305470p.
[34] O.C. Andronesi, M. von Bergen, J. Biernat, K. Seidel, C. Griesinger, E. Mandelkow, M. Baldus, Characterization of Alzheimer's-like paired helical filaments from the core domain of tau protein using solid-state NMR spectroscopy, J. Am. Chem. Soc. 130 (2008) 5922–5928, https://doi.org/10.1021/ja7100517.
[35] A.W.P. Fitzpatrick, B. Falcon, S. He, A.G. Murzin, G. Murshudov, H.J. Garringer, R.A. Crowther, B. Ghetti, M. Goedert, S.H.W. Scheres, Cryo-EM structures of tau filaments from Alzheimer's disease, Nature 547 (2017) 185–190, https://doi.org/10.1038/nature23002.
[36] B. Falcon, W. Zhang, A.G. Murzin, G. Murshudov, H.J. Garringer, R. Vidal, R.A. Crowther, B. Ghetti, S.H.W. Scheres, M. Goedert, Structures of filaments from Pick's disease reveal a novel tau protein fold, Nature (2018), https://doi.org/10.1038/s41586-018-0454-y.
[37] M. Margittai, R. Langen, Side chain-dependent stacking modulates tau filament structure, J. Biol. Chem. 281 (2006) 37820–37827, https://doi.org/10.1074/jbc.M605336200.
[38] M. Margittai, R. Langen, Template-assisted filament growth by parallel stacking of tau, Proc. Natl. Acad. Sci. U. S. A. 101 (2004) 10278–10283, https://doi.org/10.1073/pnas.0401911101.
[39] G. Ramachandran, J.B. Udgaonkar, Difference in fibril core stability between two tau four-repeat domain proteins: a hydrogen–deuterium exchange coupled to mass spectrometry study, Biochemistry 52 (2013) 8787–8789, https://doi.org/10.1021/bi4014352.
[40] L. Li, M. von Bergen, E.-M. Mandelkow, E. Mandelkow, Structure, stability, and aggregation of paired helical filaments from tau protein and FTDP-17 mutants probed by tryptophan scanning mutagenesis, J. Biol. Chem. 277 (2002) 41390–41400, https://doi.org/10.1074/jbc.M206334200.
[41] M. von Bergen, S. Barghorn, S. a Müller, M. Pickhardt, J. Biernat, E.-M. Mandelkow, P. Davies, U. Aebi, E. Mandelkow, The core of tau-paired helical filaments studied by scanning transmission electron microscopy and limited proteolysis, Biochemistry 45 (2006) 6446–6457, https://doi.org/10.1021/bi052530j.
[42] M.J. Cannon, A.D. Williams, R. Wetzel, D.G. Myszka, Kinetic analysis of beta-amyloid fibril elongation, Anal. Biochem. 328 (2004) 67–75, https://doi.org/10.1016/j.ab.2004.01.014.
[43] T. Gurry, C.M. Stultz, Mechanism of amyloid-β fibril elongation, Biochemistry 53 (2014) 6981–6991, https://doi.org/10.1021/bi500695g.
[44] N. Schwierz, C.V. Frost, P.L. Geissler, M. Zacharias, Dynamics of seeded Aβ40-fibril growth from atomistic molecular dynamics simulations: kinetic trapping and reduced water mobility in the locking step, J. Am. Chem. Soc. 138 (2016) 527–539, https://doi.org/10.1021/jacs.5b08717.
[45] W.P. Esler, E.R. Stimson, J.M. Jennings, H.V. Vinters, J.R. Ghilardi, J.P. Lee, P.W. Mantyh, J.E. Maggio, Alzheimer's disease amyloid propagation by a template-dependent dock-lock mechanism, Biochemistry 39 (2000) 6288–6295, https://doi.org/10.1021/bi992933h.